Compensated bismuth-loaded plastic scintillators for neutron detection using low-energy pseudo-spectroscopy

Jonathan Nicolas Dumazert, Romain Coulon, Guillaume H. V. Bertrand, Stéphane Normand, Laurence Méchin, Matthieu Hamel

Compensated bismuth-loaded plastic scintillators for neutron detection using low-energy pseudo-spectroscopy

Jonathan Dumazert[a], Romain Coulon[a], Guillaume H.V.Bertrand[a], Stéphane Normand[a], Laurence Méchin[b], Matthieu Hamel[a]

[a] CEA, LIST, Laboratoire Capteurs Architectures Electroniques, 91191 Gif-sur-Yvette, France

[b] CNRS, UCBN, Groupe de Recherche en Informatique, Image, Automatique et Instrumentation de Caen, 14050 Caen, France

Abstract

Gadolinium-covered modified plastic scintillators show a high potential for the deployment of cost-effective neutron detectors. Taking advantage of the low-energy photon and electron signature of thermal neutron captures in gadolinium-155 and gadolinium-157 however requires a background correction. In order to display a trustable rate, dual compensation schemes appear as an alternative to Pulse Shape Discrimination. This paper presents the application of such a compensation scheme to a two-bismuth loaded plastic scintillator system. A detection scintillator interacts with incident photon and fast neutron radiations and is covered with a gadolinium converter to become thermal neutron-sensitive as well. In the meantime, an identical compensation scintillator, covered with terbium, solely interacts with the photon and fast neutron part of incident radiations. After the acquisition and the treatment of the counting signals from both sensors, a hypothesis test determines whether the resulting count rate after subtraction falls into statistical fluctuations or provides a robust image of neutron activity. A laboratory prototype is tested under both photon and neutron radiations, allowing us to investigate the performance of the overall compensation system. The study reveals satisfactory results in terms of robustness to a cesium-137 background and in terms of sensitivity in presence of a californium-252 source.

Keywords

Neutron detection, Compensation, Modified plastic scintillators

1. Introduction

Detecting neutron radiation is vital in numerous fields of nuclear instrumentation, from flow monitoring on industrial infrastructures [1] to dose rate assessment for radioprotection [2], and notably to address radiological threats in homeland security [3]. Alternative technologies to conventional helium-3 detectors are actively searched for due to the worldwide strategical issues surrounding tritium and the repeatedly announced shortage of the isotope [4]. In this context, the interest in the loading of plastic scintillators with organometallic complexes has risen, as compatible with the deployment of sensitive, scalable and cost-effective detectors [5]. Bismuth has thus been extensively studied [6], [7] as a dopant for low and medium-energy gamma-ray pseudo-spectroscopy. Now the use of gadolinium, which exhibits the largest cross-section (48,890 b) available among stable elements for the capture of incident thermal neutrons,

in conjunction with bismuth-loaded plastic scintillators opens a potential for innovation. A technical conundrum lies within the separation of the scintillation signal due to the prompt gamma-rays most significantly emitted after the (n,γ) neutron radiative capture from the scintillation signal attributable to ambient gamma-rays and falling into the same energy range. To address this limitation, the authors propose a two-scintillator neutron detection system using a dual gadolinium/terbium detection and compensation scheme.

2. Related work

Neutron detection represents a long-term technological challenge due to the indirectly ionizing nature of the radiation: the secondary particles generated after an interaction between a neutron and an atom of the sensor, which carry a charge, actually form the signature of the neutron presence. It is also imperative, when monitoring neutron activity, to discriminate this signature against the signal generated by secondary particles generated through the interaction between background photon radiation and the electrons of the sensor atoms. Among the detectors specifically dedicated to thermal neutrons, helium-3 counters, which exploit a (n,p) type reaction with a thermal cross-section equal to 5327 b, are the most widespread [8]. Given the massive market value fluctuations of helium-3, alternative technologies are investigated, notably among scintillators [9].

In order to increase their sensitivity to thermal neutron radiations, these plastics have to be loaded with neutron adsorbing dopants, mainly boron-10 or lithium-6 [10], [11], [12]. While these isotopes, as alpha particles emitters after neutron capture, allow a discrimination by the difference in deposited energy densities between neutron and photon-generated pulses (the background photon signature being essentially formed of low-energy electrons and photons), their absorption thermal cross-section, respectively equal to 3840 and 950 b, is significantly lower than the one of their helium-3 competitor. A real time neutron radioactivity monitoring system based on these isotopes would additionally require the electronic embedment of online Pulse Shape Discrimination (PSD) algorithms.

As already mentioned, natural gadolinium presents a 48,890 b cross-section for the radiative (n,γ) capture of thermal neutrons [13] at 25 meV (ambient temperature), hence qualifying it as a sensitive neutron radiation converter. Two main approaches have been explored in order to take advantage of this capture efficiency. The insertion of gadolinium inside the sensor was investigated in the fields of inorganic scintillation, as in Lithium–Gadolinium-Borate crystals [14] and gadolinium-loaded hafnium oxide [15], and modified-plastic scintillation, for instance by the loading of a polystyrene matrix with gadolinium tris-tetramethylheptanedionate complexes [16]. The most common approach nevertheless remains, out of feasibility and reproducibility considerations, the covering of a photon radiation sensor with a gadolinium layer, therefore exploiting the electron and photon cascade after thermal neutron capture as a signature for the detection. Gadolinium-covered gas detectors have been extensively studied by Abdushukurov et al. [17] while Masaoka et al. [18] have developed a micro-strip gas chamber equipped with a gadolinium converter for neutron-position sensitive detection associated with scattering experiments.

With the aim of developing robust and portable detectors for personal operational dosimetry, semiconductor-based technologies are privileged, due notably to their high electron stopping power and photon attenuation, together with superior spectroscopic performance. Vitale et al. [19] have thus validated the patented concept of a solid-state neutron detector with a gadolinium converter through neutron beam exposures, while gadolinium covers have been inserted into

MOSFET components as reported by Lee et al. [20]. Pixelated gadolinium-covered cadmium telluride diodes have similarly been assessed by Miyake et al. [21] with the purpose of taking advantage of both the cadmium and the gadolinium high cross-sections for thermal neutron captures.

As the essential part of the exploitable prompt photon and electron signature reads under 200 keV for portable sensors [22], a major technical difficulty lies within the separation of the scintillation signal attributable to recoil electrons in the plastic matrix, generated after an interaction with electrons or photons present in the (n,γ) cascade, from secondary electrons due to an interaction with background photons of comparable energy. This issue is addressed in reference work by the implementation of various two-sensor compensation schemes. Kandlakunta et al. [23] have introduced a head-to-tail two-silicon semiconductor system to quantify the internal conversion electrons produced after a neutron radiative capture. Both semiconductors are covered with a 25 µm gadolinium foil, and a High Density Polyethylene (HDPE) layer stops the internal conversion electrons at the entrance of one of the two sensors. The substraction of both sensor responses therefore only restitutes the electron signature of incident thermal neutron captures. Aoyama et al. [24] have described another two-silicon semiconductor compensation scheme, in which two distinct covers are used: a gadolinium cover for the first detector and a tin one, chosen for its atomic number (Z = 50) reasonably close to the one of gadolinium (Z = 64), for the second detector. A 2 mm Lucite layer is used to isolate the electron responses of both sensors to incident radiations, the substraction of both spectral responses aiming at highlighting 71 keV internal conversion electrons emitted after neutron radiative captures.

This paper describes the investigation of a plastic-scintillator based alternative to semiconductors in two-sensor compensation schemes. In order to maximize the detection efficiency of the system, the entire photon and electron capture signature below 200 keV is exploited, which no longer requires a 10 keV energy resolution (like in the isolation of internal conversion electrons). In these conditions, the pseudo-spectroscopic performance of moderate-size bismuth-loaded plastic scintillators offers sufficient detection efficiency and energy resolution at low and medium energies. Additionnally, the detection of the prominent gamma-ray and internal conversion electron signature below 200 keV is enhanced by the closest compensation available of the interactions between the gadolinium converter and incident photon radiations, which is ensured by a terbium-based correction. The concomitant gain in robustness and sensitivity will allow us, after the adequate treatment of the counting signals, to present quantitative figures of merit for the detection of incident neutron radiations.

3. Principle of the detection method

The principle of the neutron radiation detection system hereby presented is based on three key features:

1) The use of a natural gadolinium cover on scintillator sensor to convert incident thermal neutron radiation into a photon (prompt gamma-rays and X-rays) and electron (internal conversion and auger electrons) source term;

2) a two-identical bismuth-loaded plastic scintillator system, where:

- the first scintillator, named *detection scintillator*, is covered with a gadolinium foil in which incident thermal neutron absorption occurs, while both the scintillator and the foil interact with incident photon radiation (and more marginally incident fast neutrons);

- the second scintillator, named *compensation scintillator*, is covered with a terbium foil of the same thickness as the gadolinium one. Both the scintillator and the foil interact with the photon and fast neutron part of the incident radiation, while thermal neutron absorption in terbium is negligible.

As, contrary to reference work [23], [24], we aim at exploiting the photon part of the neutron capture signature, the cover of the compensation detector must present the closest behavior to gadolinium (atomic number Z = 64) regarding photoelectric effects, Compton diffusions and X-ray emissions, which no element ensures more finely than terbium (Z = 65). In order to select energy windows of interest when studying the response to radiations, the sensors must allow for low-energy pseudo-spectroscopy through the enhancement of photoelectric and Compton interactions, hence the incorporation of bismuth in the scintillators;

3) a unit for the compensation treatment of the signals collected on both channels, which isolates the signature of the interaction between thermal neutrons and gadolinium in the detection scintillator by subtracting the compensation scintillator response (incident photon and fast neutron radiations) to the total detection scintillator response (incident photon, fast and slow neutron radiations).

3.1. Photon and electron signature of thermal neutron radiative capture by gadolinium-157 and gadolinium-155 isotopes

Natural gadolinium (Gd) exists in the form of a combination of isotopes among which gadolinium-155 (14.8% proportion, 60,900 b cross-section) and mostly gadolinium-157 (15.65%, 254,000 b) present an exceptionally high interaction probability with thermal neutrons [13].

The prompt source term associated with the de-excitation of a gadolinium nucleus after the absorption of a thermal neutron is subdivided into a prompt photon source term and a prompt electron source term. The complete equations of the nuclear reactions are presented in Eqs. (1) and (2), where the sum of the gamma rays labeled γ and the X-rays noted *RX* forms the photon source term, and the sum of internal conversion electrons noted CIe^- and the Auger electrons labeled Ae^- forms the electron source term.

$$^{155}_{64}Gd + {}^{1}_{0}n \rightarrow {}^{156}_{64}Gd^* + \gamma + RX + CIe^- + Ae^- \qquad (1)$$

$$^{157}_{64}Gd + {}^{1}_{0}n \rightarrow {}^{158}_{64}Gd^* + \gamma + RX + CIe^- + Ae^- \qquad (2)$$

As we primarily aim at deploying small and medium-volume scintillators (1–10 cm height and diameter), the exploitable signature is limited to the most significant electron terms and few hundred keV photon terms, which will significantly interact inside the sensors and thus induce a measurable scintillation signal. For the $^{157}_{64}Gd\ (n,\gamma)$ radiative capture, the significant γ are emitted at 79.51 keV (0.773 per neutron capture hereafter abbreviated nc) and 181.931 keV (1.39/nc) [25], together with the significant CIe^- associated with the lowest energy ray at 29.27 keV (0.348/nc) [26] and accompanying *RX* [25] between 5 and 50 keV. For the $^{155}_{64}Gd$ radiative capture, the significant γ are emitted at 88.967 keV (0.266/nc) and 199.213 keV (0.389/nc) [25], together with the significant CIe^- associated with the lowest energy ray ray at 38.73 keV (0.107/nc) [26] and accompanying *RX* [25] between 5 and 50 keV.

A characteristic spectral distribution of the statistical signature of a thermal neutron flux into a gadolinium-covered bismuth-loaded plastic scintillator is simulated using the probabilistic MCNPX2.7 Monte Carlo code for particle transport [27]. The program simulates a complete history of every generated corpuscle, for source terms as well as for diffusion products, until its energy falls below a 1 keV threshold.

The modeled natural gadolinium converter takes the simplified form of a 100% pure 7.901 g/cm^3 density foil whose thickness is set equal to 250 µm. The bismuth-loaded plastic scintillator is represented by a 1.1 g/cm^3 84.6 wt% carbon, 7.1 wt% hydrogen, 6.2 wt% oxygen, 1.3 wt% nitrogen and 0.8 wt% bismuth, $h = 2.9$ cm height and $r = 3.3$ cm radius perfect cylinder using the MCNPX2.7 benz.01t material card to account for the styrene structure of the matrix. The diffusers described in paragraph *III.B.* are neglected in this first-order model.

For gadolinium-155 and 157 isotopes respectively, a photon and electron source term following a homogenous spatial distribution is generated inside the converter using the IAEA database [25] for the totality of the prompt gamma-rays and the BRICC database [26] for the main internal conversion electrons with associated X rays and Auger electrons. Eventually, using the deposition pulse height tally 8 of the MCNPX2.7 code, the spectrum of photon and electron actual energy deposition inside the bismuth-loaded plastic scintillator is calculated. These rates are respectively labeled $\tau_{D,157}$ and $\tau_{D,155}$ for the de-excitation source terms associated with gadolinium-157 and 155, and expressed in deposition probability per source term (d.t^{-1}).

The overall τ typical spectrum for the signature deposition for the detection reads

$$\tau = \frac{\alpha.\tau_{D,157} + \beta.\tau_{D,155}}{\alpha+\beta} \qquad (3)$$

with the α and β weighting coefficients being computed as the products of isotopic importance and cross-section.

The spectral distribution displayed in Fig. 1 confirms that the energy deposition from the de-excitation signature predominantly lies under 200 keV, with peaks corresponding to the couple of gamma-rays, internal conversion electrons and X rays highlighted *supra*.

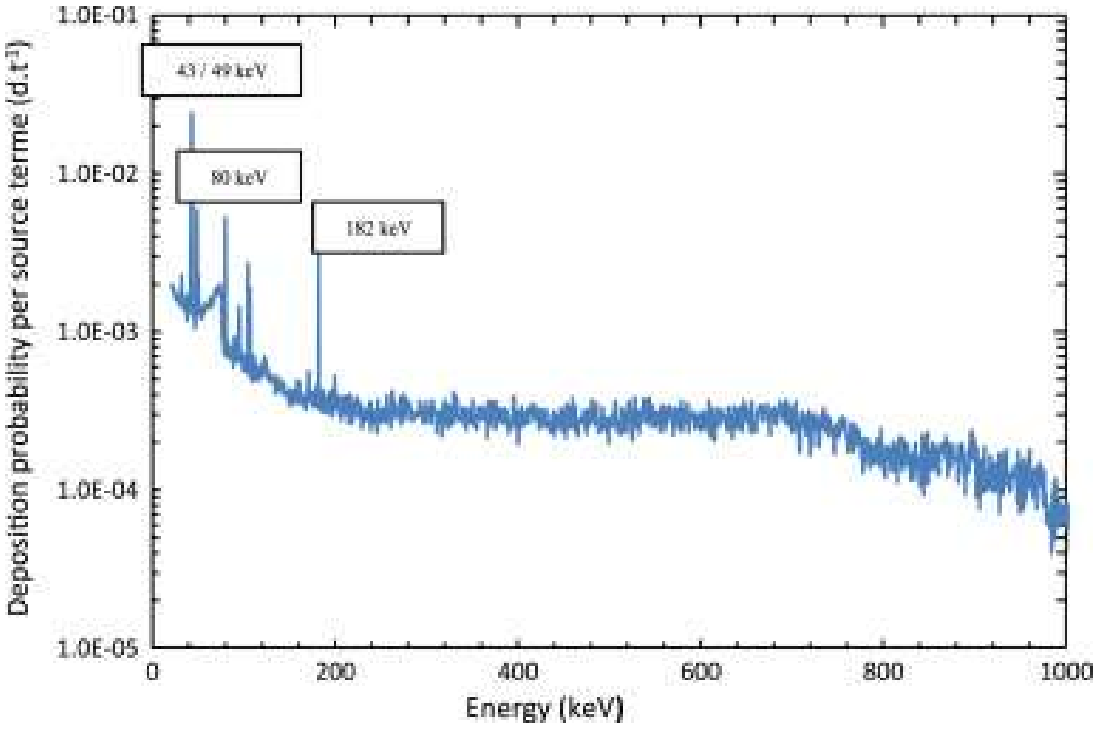

Fig. 1. Simulated spectral distribution of the capture signature in a 0.8 wt% bismuth-loaded plastic scintillator.

3.2. Detail of the system

The detection and compensation part of the device is represented by two same-geometry equal-volume plastic scintillators, which may be set side by side as presented in Fig. 2 or head to tail. The detection scintillator (1) is covered with gadolinium (3) under the form of a metal, oxide or alloy foil or deposit, whereas the compensation scintillator (2) is covered with terbium (4) (or failing that any alternative lanthanide with the closest atomic number to the one of gadolinium), with the same possible options. Both scintillators are covered with diffusers (5) such as white paint or Teflon so that as many scintillation photons as possible are collected. Both channels are isolated by a suitably dimensioned attenuator (typically lead) thickness (6) inserted in between them so that X and gamma rays generated inside (3) and forming the exploited signature of a neutron capture induce as few false counts in (2) as possible. Both scintillator plus converter ensembles may optionally be isolated from photon background radiation by a lead or steel shield (7), in order to maximize the signal-to-noise ratio, completed by a moderating material for incident neutrons such as a thickness of polyethylene, and a mu-metal shield against static magnetic fields. The conversions of the scintillation photons from (1) and (2) are respectively performed at the entrances of the photomultipliers (8) and (9). The acquisition and compensation treatment of the electronic signals from (8) and (9) is achieved by dedicated electronics (10) connected to a software and interface (11).

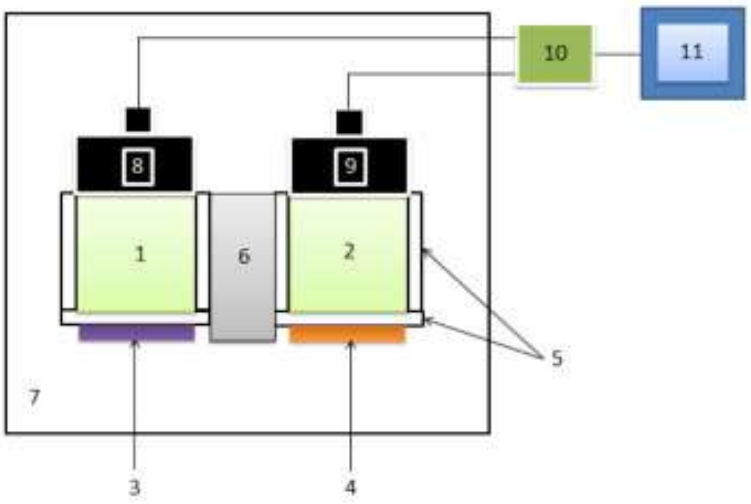

Legend:
1: Detection bismuth-loaded plastic scintillator
2: Compensation bismuth-loaded plastic scintillator
3: Gadolinium cover
4: Terbium cover
5: White paint reflector
6: Lead isolator
7: Shield / moderator
8: Photomultiplier tube
9: Photomultiplier tube
10: Electronic chain
11: Software and interface

Fig. 2. Principle sketch of the detection system.

The treatment of scintillation pulses includes amplitude triggering, bin-to-bin subtraction of the energy spectra acquired on the detection channel (channel 1) and the compensation channel (channel 2), integration of the spectral difference over energy windows of interest in order to isolate the signature of thermal neutron captures in the detection scintillator. The construction and parameterization of the hypothesis test for neutron detection is thoroughly described in Section 6.

4. Elaboration of a laboratory prototype

4.1. Preparation of bismuth-loaded plastic scintillators

The loading of plastic scintillators remains arduous as far as turbidity, self-absorption, stability and homogeneity may be concerned [28]. For the assessment of the detection method described *supra*, bismuth-loaded plastic scintillators are prepared as described by Bertrand et al. [16] and comprise:

1. a reticulated polystyrene matrix;
2. 2,5-diphenyloxazole (PPO) as a primary fluorophore;
3. 1,4-Bis((2-methylstyryl)benzene) (Bis-MSB) as a secondary fluorophore;

4. triphenyl bismuth ($BiPh_3$) as a bismuth-rich organometallic compound.

The topological representation of these molecules is presented in Fig. 3. The choice of a styrene-based matrix is firstly driven by commercial standard, cost-effectiveness and radiation hardness [29]. It is secondly noteworthy that, though bismuth has been successfully inserted in polyvinylcarbazole (PVK) matrices [30], these are challenging in terms of scalability, process (high temperature being required for polymerization), temperature and mechanical resilience. An extensive study of tricarboxylate and triaryl organometallic compounds in polystyrene-based scintillators [31] has shown that $BiPh_3$ significantly enhances photoelectric effects below 200 keV, which is critical for low-energy pseudo-spectroscopy, without inducing any dramatic scintillation quenching when inserted up to 17 wt%. A proof of scalabity up to 155 cm^3 for a 5 wt% bismuth load was additionally established in [16], which will be exploited in future developments.

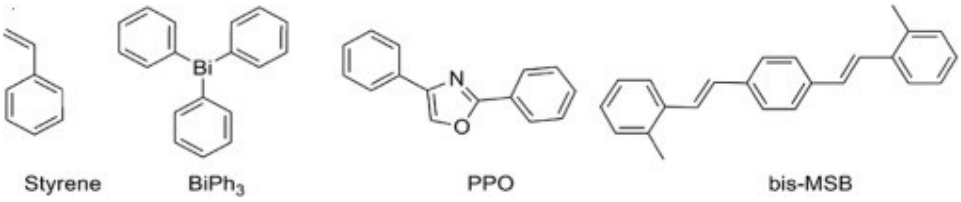

Fig. 3. Topological representation of molecules.

All the components were mixed in a round bottom flask. The resulting solution was put under a nitrogen atmosphere and then frozen using liquid nitrogen. Multiple freeze–pump–thaw cycles were performed to achieve total degassing. The solution was subsequently poured into a cylindrical glass mold containing a small quantity of initiator. The filled mold was purged with nitrogen, sealed and placed into an oven at 40–45 °C for 30 days. Once complete polymerization was observed, the mold was cooled down to room temperature and shattered to free the plastic piece.

The quantitative composition of bismuth-loaded plastic scintillators is described in Table 1: based on the conclusions of [16], the authors have inserted the largest assessed quantity of primary fluorophore for given monomer and organometallic dopant quantities in order to maximize the light yield. A 0.8 wt% bismuth load was selected to allow for a scale-up from the reference samples (2 cm^3 as exploited for neutron detection in [22]) without any dramatic degradation of the homogeneity nor of the optical qualities of the prototype sensor.

$m_{monomers}$ (g)	m_{PPO} (g)	$m_{Bis\text{-}MSB}$ (mg)	m_{dopant} (mg)	wt% (Bi)
13.44	4.14	5.4	420 ($BiPh_3$)	0.8

Table 1. Composition of bismuth-loaded plastic scintillators

The scintillating samples are cut into a cylindrical shape and polished so that they meet the desired dimensions, i.e. 3.3 cm diameter and 2.9 cm height. Their lateral surface is ultimately covered with a reflecting white paint to limit the escape of scintillation photons.

The most crucial figure of merit for the employability of the synthetized scintillators as radioactivity sensors lies within their light yield, labeled R_{ph} and expressed in scintillation photon per megaelectronvolt (Ph/MeV). This yield is determined by a relative method, using

the acquisition and measurement setup described in the next paragraph, where the high voltage is set equal to 1700 V, successively with our 0.8 wt% bismuth-loaded plastic scintillator and an identical shape and volume reference EJ-200 whose yield is known to equal $R_{ph} = 10000 \pm 100\ Ph/MeV$. Both samples are exposed to a cesium-137 source of activity $A = 34$MBq for 10 min. The ratio of the channel numbers corresponding to 80% of the Compton maxima provides a value for the relative yield of our sample to the reference. A light yield $R_{ph} = 8500 \pm 200\ Ph/MeV$ is derived for the 0.8 wt% bismuth-loaded plastic scintillator, qualifying it as a decent candidate for gamma-ray detection. The ultraviolet (UV) responses of the scintillators are depicted in Fig. 4, while their spectral responses to the cesium-137 exposure are superimposed in Fig. 5.

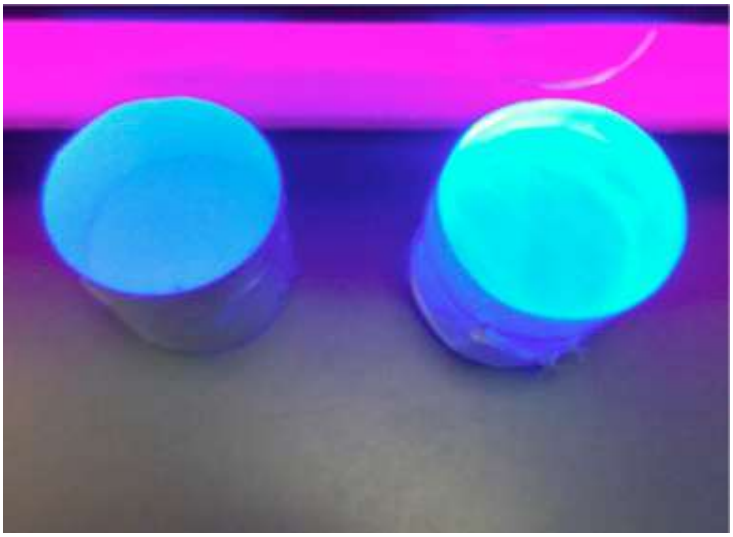

Fig. 4. UV responses of 0.8 wt% bismuth-loaded plastic scintillator (left) and reference EJ-200 (right).

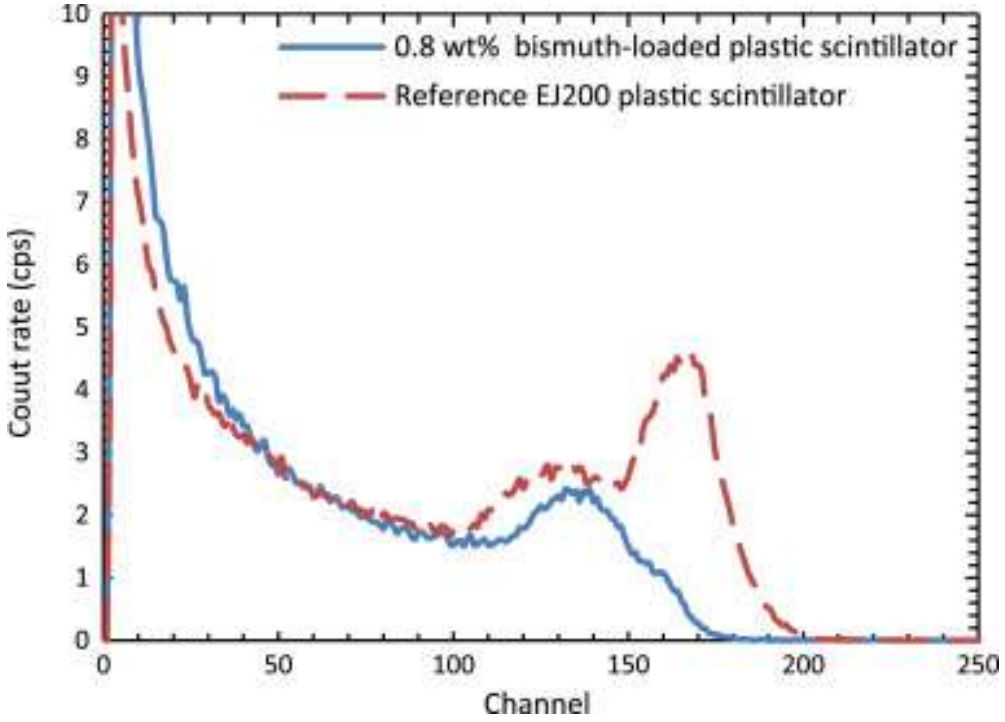

Fig. 5. Energy spectra of 0.8 wt% bismuth-loaded plastic scintillator and reference EJ-200 in presence of a cesium-137 source.

4.2. Acquisition and measurement setup

On both the detection and compensation channel, the uncovered face of the plastic scintillator is coupled to a bialkali photocathode of a Hamamatsu™ H1949-51 model photomultiplier tube (PMT) powered by a CAEN N147 model 4CH HV programmable power supply. A custom made electronic card developed at the CEA LIST [32] and devoted to the processing of short scintillation pulses (rise and decay time within the nanosecond time scale) digitizes the signal at a frequency equaling 200 Msample s^{-1}, performs a filtering of the signal over 7 samples in order to maximize the signal-to-noise ratio (SNR) and a differentiation to correct base line fluctuations, triggers the pulse and determines its maximal amplitude to store the event into a 8-bit pulse height histogram. The PMT is isolated from ambient light and static noise sources inside an opaque Faraday cage.

5. Energy calibration of the plastic scintillators

In order to implement a counting compensation over energy windows of interest below 200 keV, it is necessary, for the bismuth-loaded samples, to establish a correspondence between every channel in which counts are displayed and an energy value. An energy calibration of the scintillators was performed by making use of several gamma radiation sources available in the laboratory, positioned at a distance $d = 1.5$ cm of the scintillator surface along the symmetry axis of the scintillator:

- an *americium-241* source whose photoelectric peak is observed at 59 keV;
- a *cobalt-57* source whose photoelectric peak is observed at 122 keV;

– an *europium-152* source with one photoelectric peak observed at 122 keV, and two Compton edges respectively at 198 keV and 245 keV.

The experimental points are joined by line segments. The three counting spectra are superimposed on Fig. 6, whereas Fig. 7 presents the energy calibration curve.

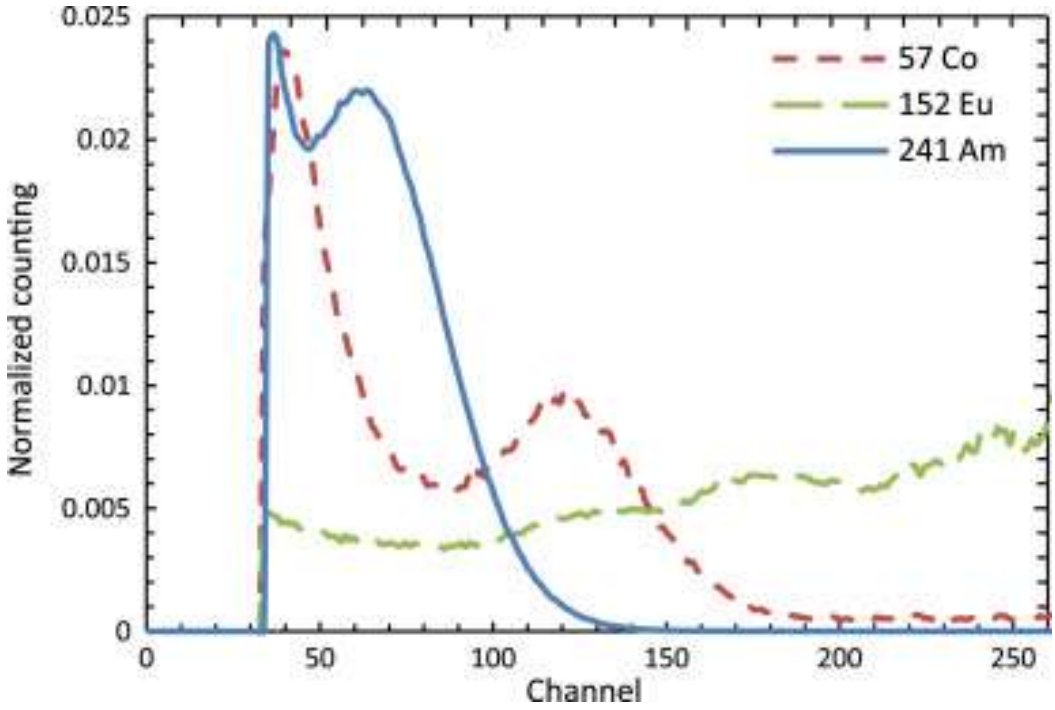

Fig. 6. Energy spectra in presence of americium-241, cobalt-57 and europium-152 sources.

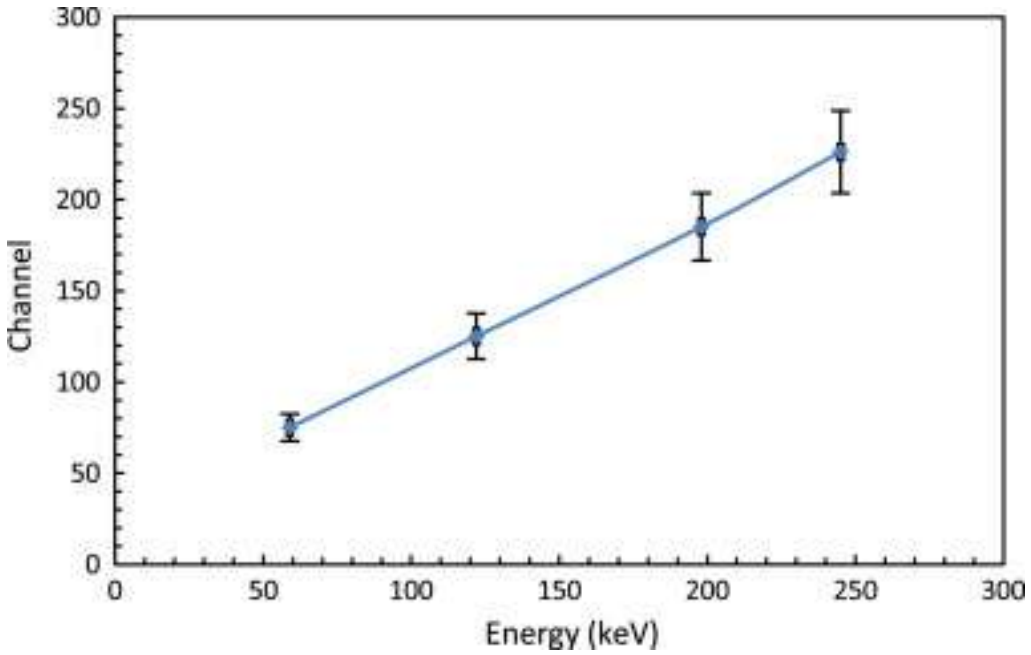

Fig. 7. Energy calibration curve of bismuth-loaded plastic scintillator.

6. Hypothesis test for neutron detection

From the counts N_1 and N_2, collected on channel 1 (gadolinium-covered detection scintillator) and 2 (terbium-covered compensation scintillator) respectively, and integrated over a temporal window τ (empirically identified as sufficient to achieve precise and stable count rate estimations), it is easy to compute the average count rates noted $\widehat{\lambda_1}$ and $\widehat{\lambda_2}$, by Eq. (4) and Eq. (5), as well as their associated standard deviations $\sigma\left(\widehat{\lambda_1}\right)$ and $\sigma\left(\widehat{\lambda_2}\right)$ according to Eq. (6) and Eq. (7).

$$\widehat{\lambda_1} = \frac{N_1}{\tau} \qquad (4)$$

$$\widehat{\lambda_2} = \frac{N_2}{\tau} \qquad (5)$$

$$\sigma\left(\widehat{\lambda_1}\right) = \sqrt{\frac{\widehat{\lambda_1}}{\tau}} \qquad (6)$$

$$\sigma\left(\widehat{\lambda_2}\right) = \sqrt{\frac{\widehat{\lambda_2}}{\tau}} \qquad (7)$$

The neutron detection operation takes the form of a classical hypothesis test with a null hypothesis $\mathbf{H}_0$ representing the absence of any detected neutron activity and the non-null hypothesis $\mathbf{H}_1$ representing the detection of a neutron activity. The test compares the difference of the count rates estimated on channel 1 and 2 respectively to a significance level which is proportional to the standard deviation of the difference.

If:

$$\widehat{\lambda_1} - \widehat{\lambda_2} > t_K \bullet \sqrt{\sigma^2\left(\widehat{\lambda_1}\right) + \sigma^2\left(\widehat{\lambda_2}\right)} \qquad (8)$$

Then $\mathbf{H}_1$ is accepted.

Else $\mathbf{H}_0$ is accepted with a confidence level $1 - K$.

The coverage factor t_K in hypothesis test Eq. (8) for neutron detection governs the thermal neutron sensitivity $S_n$versus false detection probability K compromise. The distributions $K = f(t_K)$ admits the well known distribution represented in Fig. 8. To ensure a $1 - K = 95\%$ $c$onfidence level, the coverage factor is set equal to $t_K = 1.96$. Eventually, in case $\mathbf{H}_1$ is accepted, a rate labeled $\widehat{\lambda_n}$, attributable to thermal neutrons incident on the detection channel and captured in the gadolinium cover, is estimated over the temporal window τ as

$$\widehat{\lambda_n} = \left(\widehat{\lambda_1} - \widehat{\lambda_2}\right) \pm \sqrt{\sigma^2\left(\widehat{\lambda_1}\right) + \sigma^2\left(\widehat{\lambda_2}\right)} \qquad (9)$$

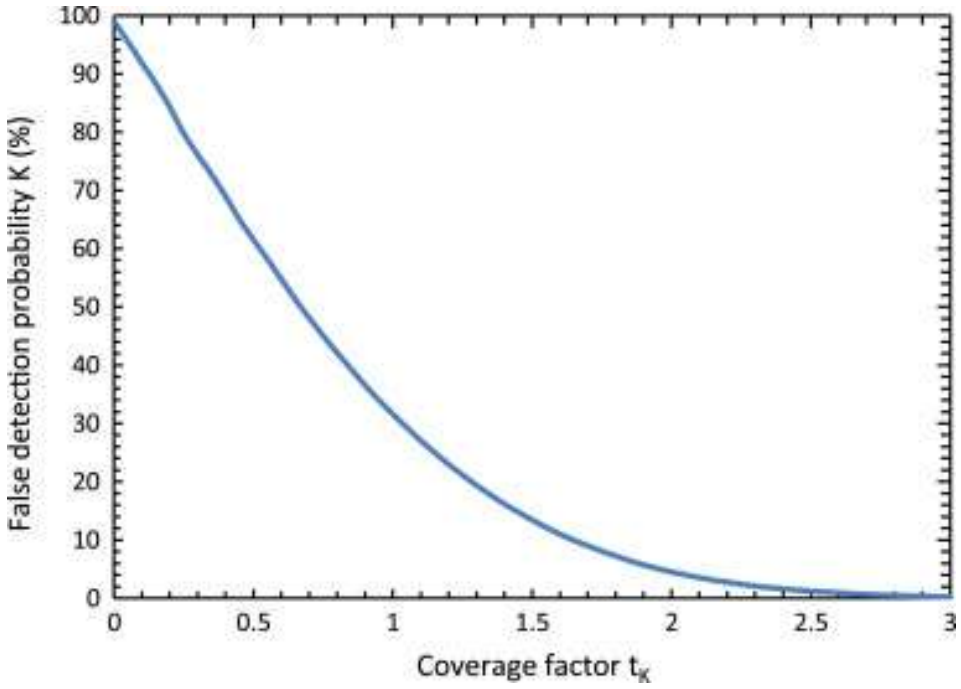

Fig. 8. Distribution of the false detection probability K as a function of the coverage factor t_K.

7. Results

In order to assess the performance of the detection scheme described throughout the previous sections, three counting measurements were performed on channels 1 and 2:

- radiation measurement over $\tau = 900$ s in presence of a *cesium-137* source of activity $A = 34$ MBq positioned at a distance $d = 16$ cm of the detection ensemble along its symmetry axis;
- radiation measurement over $\tau = 3600$ s in presence of a *californium-252* source of activity $A = 784$ kBq positioned at a distance $d = 16$ cm of the detection ensemble with $e = 5$ cm High Density Polyethylene (HDPE) neutron moderator in between;
- radiation measurement over $\tau = 3600$ s in presence of a *californium-252* source of activity $A = 784$ kBq positioned at a distance $d = 16$ cm of the detection ensemble with $e = 5$ cm Permali HB 780 boron wood neutron moderator and absorber in between.

Both gadolinium and terbium covers are 2.5×2.5 cm surface 250 µm thick 99.9% pure metal foils from Strem Chemicals [33], [34]. The scintillators are isolated by a 5 cm thick lead shield. No lead castle against background photon radiation was added to the setup. The high voltage supplying the photomultipliers is set equal to 2000 V.

The average count rates $\widehat{\lambda_1}$ and $\widehat{\lambda_2}$ computed over selected energy windows of interest are listed in Table 2. The relevant quantities for the detection test as well as the result of the said test are reported in Table 2. The experimental setup (detection channel) is depicted in Fig. 9 in presence of a californium-252 source plus boron wood exposure.

Energy range/radiation background	Cesium-137	Californium-252+HDPE	Californium-252+boron wood
[59 keV-max]	$\widehat{\lambda_1} = 979.13 \pm 0.74$	$\widehat{\lambda_1} = 130.22 \pm 0.11$	$\widehat{\lambda_1} = 98.61 \pm 0.10$
	$\widehat{\lambda_2} = 980.62 \pm 0.74$	$\widehat{\lambda_2} = 129.83 \pm 0.11$	$\widehat{\lambda_2} = 99.04 \pm 0.10$
	$\widehat{\lambda_1} - \widehat{\lambda_2} = -1.49$	$\widehat{\lambda_1} - \widehat{\lambda_2} = 0.39$	$\widehat{\lambda_1} - \widehat{\lambda_2} = -0.43$
	$t_K \bullet \sqrt{\sigma^2(\widehat{\lambda_1}) + \sigma^2(\widehat{\lambda_2})} = 1.45$	$t_K \bullet \sqrt{\sigma^2(\widehat{\lambda_1}) + \sigma^2(\widehat{\lambda_2})} = 0.30$	$t_K \bullet \sqrt{\sigma^2(\widehat{\lambda_1}) + \sigma^2(\widehat{\lambda_2})} = 0.27$
	$\mathbf{H_0}$ accepted	$\mathbf{H_1}$ accepted	$\mathbf{H_0}$ accepted
		$\widehat{\lambda_n} = 0.39 \pm 0.16$	
[122 keV-max]	$\widehat{\lambda_1} = 798.34 \pm 0.67$	$\widehat{\lambda_1} = 88.00 \pm 0.09$	$\widehat{\lambda_1} = 64.78 \pm 0.08$
	$\widehat{\lambda_2} = 800.39 \pm 0.67$	$\widehat{\lambda_2} = 87.71 \pm 0.09$	$\widehat{\lambda_2} = 65.05 \pm 0.08$
	$\widehat{\lambda_1} - \widehat{\lambda_2} = -2.05$	$\widehat{\lambda_1} - \widehat{\lambda_2} = 0.29$	$\widehat{\lambda_1} - \widehat{\lambda_2} = -0.27$
	$t_K \bullet \sqrt{\sigma^2(\widehat{\lambda_1}) + \sigma^2(\widehat{\lambda_2})} = 1.85$	$t_K \bullet \sqrt{\sigma^2(\widehat{\lambda_1}) + \sigma^2(\widehat{\lambda_2})} = 0.25$	$t_K \bullet \sqrt{\sigma^2(\widehat{\lambda_1}) + \sigma^2(\widehat{\lambda_2})} = 0.21$
	$\mathbf{H_0}$ accepted	$\mathbf{H_1}$ accepted	$\mathbf{H_0}$ accepted
		$\widehat{\lambda_n} = 0.29 \pm 0.13$	
[198 keV-max]	$\widehat{\lambda_1} = 468.31 \pm 0.51$	$\widehat{\lambda_1} = 36.46 \pm 0.05$	$\widehat{\lambda_1} = 26.06 \pm 0.05$
	$\widehat{\lambda_2} = 468.25 \pm 0.51$	$\widehat{\lambda_2} = 36.48 \pm 0.06$	$\widehat{\lambda_2} = 26.06 \pm 0.05$
	$\widehat{\lambda_1} - \widehat{\lambda_2} = 0.06$	$\widehat{\lambda_1} - \widehat{\lambda_2} = -0.02$	$\widehat{\lambda_1} - \widehat{\lambda_2} = 0.00$
	$t_K \bullet \sqrt{\sigma^2(\widehat{\lambda_1}) + \sigma^2(\widehat{\lambda_2})} = 1.41$	$t_K \bullet \sqrt{\sigma^2(\widehat{\lambda_1}) + \sigma^2(\widehat{\lambda_2})} = 0.16$	$t_K \bullet \sqrt{\sigma^2(\widehat{\lambda_1}) + \sigma^2(\widehat{\lambda_2})} = 0.14$
	$\mathbf{H_0}$ accepted	$\mathbf{H_0}$ accepted	$\mathbf{H_0}$ accepted

Table 2. Average count rates in count per second (cps) over energy ranges of interest and results of the hypothesis test for neutron detection.

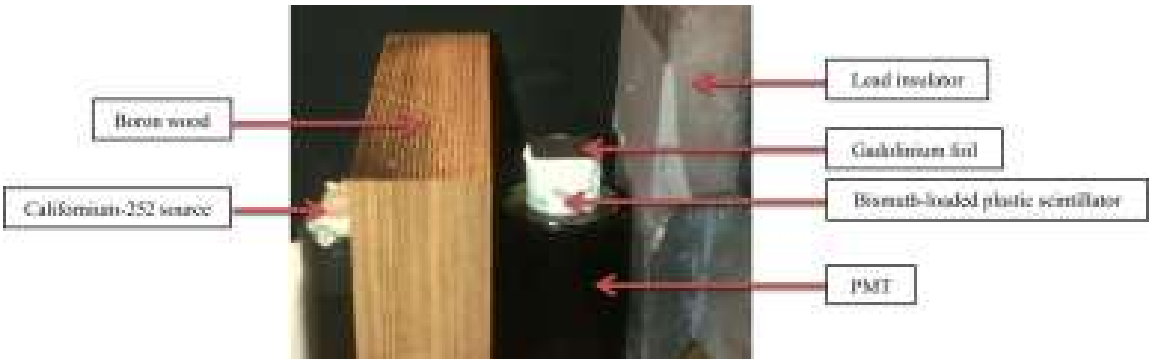

Fig. 9. Experimental measurement setup (detection channel).

8. Discussion

The neutron detection test for countings over the three considered thresholds results in a non-detection (null hypothesis acceptance) in presence of the cesium-137 source (typically used for the qualification neutron detectors as it is representative of long-lived fission products present

in the fuel cycle). The gamma dose rate at the detector level is measured equal to 17 µSv/h with a commercial Thermo Electron ESM FH 40G-L 10 radiameter, hence confirming the robustness of a photon response compensation up to "controlled area" standards, defined by legislation [35] from 7.5 to 25 µSv/h.

A sealed californium-252 source is both a neutron and a photon radiation emitter. The neutron emission is described by a Watt spectrum and associated to spontaneous fissions [36], which account for 3.09% of a californium-252 source activity. The mean number of neutrons emitted per fission equals $\nu_n = 3.77\ n/f$. This neutron emission is accompanied by a background of prompt and delayed gamma-rays (X and gamma rays associated to alpha disintegrations are neglected due to low emission probabilities for energies above 20 keV). The resultant background distribution is modeled [37] by a piecewise defined function p of photon energy E_γ, so that $p\left(E_\gamma\right) = D\ c\left(E_\gamma\right)$, where D is a normalization constant and c reads

$$c\left(E_\gamma\right) = \begin{cases} 6.6 + e^{-1.1E_\gamma}, 20\ keV < E_\gamma < 500\ keV \\ 20.2e^{-1.78E_\gamma} + e^{-1.1E_\gamma}, 500\ keV < E_\gamma < 1.4\ MeV \\ 7.2e^{-1.09E_\gamma} + e^{-1.1E_\gamma}, 1.4\ MeV < E_\gamma < 10.4\ MeV \end{cases} \quad (10)$$

The expectation for the energy of a background californium-252 gamma ray reads $\overline{E_\gamma} = 875\ keV$, which leads, in a first-order approach, to consider the compensation of a cesium-137 source (gamma emitter at 662 keV) as representative of the californium-252 photon background compensation. The gamma dose rate at the detector level in presence of the HDPE moderated californium-252 is additionally measured equal to 1.2 µSv/h with the radiometer, thus one order of magnitude below the cesium-137 background which was robustly compensated *supra*.

Now Table 2 shows that in presence of the HDPE moderated californium-252 source, the detection hypothesis is accepted when the [59–198 keV] and [122–198 keV] energy ranges are taken into account, with neutron rates reading $\widehat{\lambda_n} = 0.39 \pm 0.16$ cps and $\widehat{\lambda_n} = 0.29 \pm 0.13$ cps respectively. The detection hypothesis is however rejected for countings over a 198 keV threshold, which is consistent with the neutron capture signature distribution as presented in Fig. 1.

The neutron HDPE moderator was ultimately replaced by an identical thickness boron wood neutron moderator and absorber. The substitution firstly results in a reduction of the count rates recorded on the total considered spectra from 59 keV to saturation, for both channels considered independently. This reduction is explained by the difference in densities of the moderators, respectively $\rho_{HDPE} = 0.95$ g/cm^3 for HDPE and $\rho_{BW} = 1.35$ g/cm^3 for boron wood, and the proportionality between these densities and Compton effects in the moderating materials, responsible for the attenuation of the gamma-ray background incident on the sensors. As an illustration, the ratios of count rates recorded on [198 keV; max], with HDPE moderation and boron wood moderation read $\frac{\widehat{\lambda_{1,HDPE}}}{\widehat{\lambda_{1,BWn}}} = 1.40 \pm 0.01$ and $\frac{\widehat{\lambda_{2,HDPE}}}{\widehat{\lambda_{2,BWn}}} = 1.40 \pm 0.01$ on channel 1 and 2 respectively, in agreement with the ratio of the moderator densities $\frac{\rho_{BW}}{\rho_{HDPE}}$ =1.42, hence leading to an approximate 42% expectation of the photon background reduction. In the meantime, the substitution of HDPE by Permali boron wood results in the rejection of the detection hypothesis on the three countings ranges, therefore canceling the detection response over the two first energy ranges obtained for absorption-free moderation of incident neutron with HDPE. This measurement confirms that the photon background of the californium-252

was indeed compensated in the HDPE measurement, and that neutron captures in gadolinium were indeed responsible for a significant neutron rate displayed over [59 keV; max] and [122 keV; max].

It follows that the measurement campaign on gadolinium- and terbium-covered plastic scintillators highlights the potential for a robust compensation technique dedicated to neutron radiation detection, associated with selective counting at low and medium-energy allowed by bismuth-loading. In order to benchmark the thermal neutron detection scheme based on the physical sensors and the numerical parameters we have introduced, with reference helium-3 proportional counters, a thermal neutron sensitivity estimate labeled $\widehat{S_n}$ and expressed in count per thermal neutron n_{th} times square centimeter ($c/(n_{th}$ .cm^{-2}) or cps/nv) has to be calculated. The spontaneous fission rate of the californium-252 source reads

$A_{252}{}_{Cf,f} = 0.0309 \bullet A_{252}{}_{Cf} = 3.7 \bullet 10^4$ f/s expressed in fission per second, and the neutron emission rate therefore equals $A_{252}{}_{Cf,n} = 3.77 \bullet A_{252}{}_{Cf,f} = 1.4 \bullet 10^5 n/s$ expressed in neutron per second. The thermal neutron fluence incident on the detection scintillator at the exit of the HDPE moderator, i.e. the neutron fluence integrated between 1 meV and 50 meV (cadmium absorption cut-off), labeled $\Psi_{n_{th}}$ and expressed in thermal neutron per generated neutron and square centimeter ($n_{th}/(n.$ cm^2)), is evaluated by simulation using the average surface flux tally 2 of the MCNPX2.7 code. The estimate reads $\Psi_{n_{th}} = 1.6 \bullet 10^{-4}$ $n_{th}/(n.$ cm^2), from which an estimate of the thermal neutron flux incident on a sensor, labeled $\Phi_{n_{th}}$ and expressed in thermal neutron per square centimeter and per second ($n_{th}/$(cm^2 s)), is derived as

$\Phi_{n_{th}} = \Psi_{n_{th}} \bullet A_{252}{}_{Cf,n} = 5.8\ n_{th}/$(cm^2 s). The thermal neutron sensitivity estimate is eventually calculated as

$$\widehat{S_n} = \frac{\widehat{\lambda_n}}{\Phi_{n_{th}}} \qquad (11)$$

equaling $\widehat{S_n} = 0.067 \pm 0.028$ cps / nv and $\widehat{S_n} = 0.050 \pm 0.022$ cps / nv for countings over [59–198 keV] and [122–198 keV] respectively.

9. Conclusion

The neutron measurement by compensation carried out with two gadolinium- and terbium-covered bismuth-loaded plastic scintillators has allowed for the unambiguous detection of a neutron activity in the photon background of a moderated californium-252 source (estimated about 1.2 µSv/h with a standard radiameter, which matches the typical constraints of a "monitored area" in the context of radioprotection applications). Thus the concept of the neutron detection scheme introduced in this paper has been experimentally validated: this scheme has proven itself robust to a "controlled area" cesium-137 photon background, while being portable and more cost-effective than silicon-based compensation systems. In order to increase the count rates, as well as the precision associated to them, future works will be turned towards a scale-up of the loaded scintillating samples, with all the known challenges associated to such a process: homogeneity and turbidity issues with the loading, self-absorption of the scintillator. The implementation of the neutron counting scheme, including the smoothing on the acquired signals and the hypothesis test for detection, on a field-programmable gate array (FPGA) is currently under development at the CEA, LIST. Whereas preliminary simulations

have shown that ani biases result, given the relatively small dimensions of the sensors, in less than 2% distortion of the estimated count rate, this systematic bias will have to addressed by dedicated algorithms when scale-ups will be considered. Research work will additionnally be carried out on the choice of an optimal matrix and on the structuration of the scintillator-photomultiplier interface to maximize the extraction of scintillation photons.

References

[1] J.K. Mattingly, J. March-Leuba, T.E. Valentine, J.T. Mihalezo, T. Ucklan, Physics design of fissile mass-flow monitoring system, Instrumentation and Controls Division, Oak Ridge National Laboratory, 1997.

[2] D.E. Hankins, **Progress in Personal Neutron Dosimetry,** University of California, Los Alamos Scientific Laboratory, New Mexico (1973)

[3] Chemical, Biological, Radiological or Nuclear (CBRN) Detection: a Technological Overview, NATO Parliamentary Assembly, 2005, pp. 18–20.

[4] Managing Critical Isotopes, Weaknesses in DOE's Management of Helium-3 Delayed the Federal Response to a Critical Supply Shortage, GAO-11-472, U.S. Government Accountability Office, Washington, D.C., 2011.

[5] L. Pichat, P. Pesteil, J. Clément, Journal de Chimie Physique, 50 (1953), p. 26

[6] B.L. Rupert, N.J. Cherepy, B.W. Sturm, R.D. Sanner, S.A. Payne, Europhysics Letters, 97 (2012), p. 22002

[7] G.H.V. Bertrand, F. Sguerra, C. Dehé-Pittance, F. Carrel, R. Coulon, S. Normand, E. Barat, T. Dautremer, T. Montagu, M. Hamel, Journal of Materials Chemistry C, 2 (2014), p. 7304

[8] D.A. Shea, Congressional Research Service (2010)

[9] R.T. Kouzes, J.H. Ely, L.E. Erikson, W.J. Kernan, A.T. Lintereur, E.R. Siciliano, D.L. Stephens, D.C. Stromswold, R.M. Van Ginhoven, M.L. woodring, Nuclear Instruments and Methods in Physics Research Section A, 623 (2010), p. 1035

[10] G.H.V. Bertrand, M. Hamel, S. Normand, F. Sguerra, Nuclear Instruments and Methods in Physics Research Section A, 776 (2015), p. 114

[11] I.A. Pawelczak, A.M. Glenn, H.P. Martinez, M.L. Carman, N.P. Zaitseva, S.A. Payne, Nuclear Instruments and Methods in Physics Research Section A, 751 (2014), p. 62

[12] R.D. Breukers, C.M. Bartle, A. Edgar, Nuclear Instruments and Methods in Physics Research Section A, 701 (2013), p. 58

[13] D.A. Abdushukurov, **Gadolinium foils as converters of thermal neutrons in detectors of nuclear radiation,** Novinka (Ed.), Nova Science Publishers, New York (2010), p. 7

[14] A.M. Williams, P.A. Beelev, N.M. Spyrou, Radiation Protection Dosimetry, 110 (2004), p. 497

[15] B.D. Blasy, Neutron detection utilizing gadolinium doped hafnium oxide films, Department of the Air Force, 2 Lt USAF, 2008.

[16] G.H.V. Bertrand, J. Dumazert, F. Sguerra, R. Coulon, G. Corre, M. Hamel, Journal of Materials Chemistry C, 3 (2015), p. 6006

[17] D.A. Abdushukurov, M.A. Abduvokhidov, D.V. Bondarenko, K.K. Muminov, T.A. Toshov, D.Y. Chistyakov, Journal of Instrumentation, 2 (2007) PO4001

[18] S. Masaoka, T. Nakamura, H. Yamagashi, K. Soyama, Nuclear Instruments and Methods in Physics Research Section A, 513 (2003), pp. 538-549

[19] S.A. Vitale, P. Gouker, Solid-State Neutron Detector Detector with Gadolinium Converter, U.S. 2013/0056641 A1 Patent, 2013.

[20] N.H. Lee, H.J. Lee, Y.G. Hwang, S.C. Oh, G.U. Youk, IEEE Transaction on Nuclear Science, NS57 (6) (2010), p. 3489

[21] A. Miyake, T. Nishioka, S. Singh, H. Morii, H. Mimura, T. Aoki, Nuclear Instruments and Methods in Physics Research Section A, 654 (2011), p. 390

[22] J. Dumazert, R. Coulon, G.H.V. Bertrand, M. Hamel, F. Sguerra, C. Dehé-Pittance, S. Normand, L. Méchin, Compensated gadolinium-loaded plastic scintillators for thermal neutron detection and counting, in: Proceedings of the Advancements in Nuclear Instrumentation, Measurement Methods and their Applications (ANIMMA), 2015.

[23] P. Kandlakunta, L. Cao, Radiation Protection Dosimetry, 3 (2012), p. 151

[24] T. Aoyama, Y. Oka, K. Honda, C. Mori, Nuclear Instruments and Methods in Physics Research Section A, 314 (1992), p. 590

[25] 〈www-nds.iaea.org〉.

[26] 〈bricc.anu.edu.au/index.php〉.

[27] MCNPX User Manual, Los Alamos Tech. rep., LA-CP-11-00438, Los Alamos, 2011.

[28] N.J. Cherepy, R.D. Sanner, T.M. Tillotson, S.A. Payne, P.R. Beck, S. Hunter, L. Ahle, P.A. Thelin, Bismuth-loaded plastic scintillators for gamma spectroscopy and neutron active interrogation, in: Proceedings of the IEEE Nuclear Science Symposium and Medical Imaging Conference Record, 2012, pp. 1972–1973.

[29] I.G. Britvich, V.G. Vasilchenko, V.N. Kirichenko, S.I. Kuptsov, V.G. Lapshin, A.P. Soldatov, A.S. Solovev, V.I. Rykalin, S.K. Chernichenko, I.V. Shein, Instruments and Experimental Techniques, 45 (5) (2002), p. 644

[30] B.L. Rupert, N.J. Cherepy, B.W. Sturm, R.D. Sanner, S.A. Payne, Europhysics Letters, 97 (2012), p. 2

[31] G.H.V. Bertrand, F. Sguerra, C. Dehé-Pittance, F. Carrel, R. Coulon, S. Normand, E. Barat, T. Dautremer, T. Montagu, M. Hamel, Journal of Materials Chemistry C, 2 (2014), p. 7304

[32] S. Normand, V. Kondrasovs, G. Corre, K. Boudergui, N. Blanc de Lanaute, J.-M. Bourbotte, R. Woo, P. Pin, L. Tondut, IEEE Transactions on Nuclear Science, NS59 (4) (2011)

[33] 〈http://www.strem.com/catalog/v/93-6434/22/gadolinium_7440-54-2〉

[34] 〈http://www.strem.com/catalog/v/93-6519/71/terbium_7440-27-9〉

[35] Légifrance, Arrêté du 15 mai 2006 relatif aux conditions de délimitation et de signalisation des zones surveillées et contrôlées et des zones spécialement réglementées ou interdites compte tenu de l'exposition aux rayonnements ionisants, ainsi qu'aux règles d'hygiène, de sécurité et d'entretien qui y sont imposées (2006), derived from: The 2007 Recommendations of the International Commission on Radiological Protection, ICRP Publication 103, Ann. ICRP, vol. 37, 2007, pp. 2–4.

[36] Cf98252, Table de radionucléides, M.-M. Bé, V. Chisté, LNE-LNHB/CEA, 2007.

[37] R.B. Hayes, Preliminary Benchmarking Efforts and MCNP Simulation Results for Homeland, 2009, DOE/NV/25946-431, Remote Sensing Laboratory, Las Vegas, NV 89193.